ELSEVIER

Journal of Physics and Chemistry of Solids 64 (2003) 433–441

JOURNAL OF PHYSICS AND CHEMISTRY OF SOLIDS

www.elsevier.com/locate/jpcs

Lattice vibration of $Ce_{1-x}Sc_xFe_4Al_8$

Yan-mei Kang[a,*], Nan-xian Chen[a,b], Jiang Shen[b]

[a]*Department of Physics, Tsinghua University, Beijing 100084, People's Republic of China*
[b]*Institute of Applied Physics, University of Science and Technology Beijing, Beijing 100083, People's Republic of China*

Received 22 April 2002; accepted 3 July 2002

Abstract

The lattice constants of the rare earth intermetallic compounds $Ce_{1-x}Sc_xFe_4Al_8$ are calculated based on the interatomic potentials obtained by a lattice inversion method. The results are in agreement with experiments. Further, some simple mechanical properties such as the elastic constants and bulk modulus are also investigated for these materials. It is noted that, the phonon densities of states are first evaluated for the quarternary intermetallic compounds with $ThMn_{12}$-type structure and a qualitative analysis for the vibrational modes is presented. This may be an attempt to predict the mechanical and thermodynamic properties for the rare earth materials with complex structures.

Keywords: A. Intermetallic compounds; D. Crystal structure; D. Lattice dynamics; D. Mechanical properties

1. Introduction

During the past decades, the ternary Fe-rich rare-earth intermetallic compounds with the tetragonal $ThMn_{12}$ structure attracted much interest due to their higher Curie temperatures and stronger uniaxial magnetic anisotropy fields near room temperature [1–4]. Recently, a considerable attention [5–10] has been paid to the rare earth compounds RFe_4Al_8, which have the same structure and exhibit interesting magnetic properties. Neutron diffraction [7,9], Mössbauer effect [12,13] and magnetic [5,11] measurements have confirmed a complex antiferromagnetic (AF) ordering. Especially $CeFe_4Al_8$ and $ScFe_4Al_8$ compounds exhibit a long-range magnetic ordering at low temperatures due to the presence of magnetic moments on the iron sublattice [7,10]. Furthermore, Suski et al. [14] first obtained the $Ce_{1-x}Sc_xFe_4Al_8$ ($0 < x < 1$) alloys in 2000 and more detailed investigations of the magnetic and electrical properties as well as ^{57}Fe Mössbauer effect were carried out in a wide temperature range for this solid solution by Gaczyński et al. [15]. The substitution of Sc for Ce leads to a noticeable transfer of electrons between the Ce (Sc) and Fe local bands and the total effective magnetic moment decreases with the Sc content. In this work, the lattice inversion technique [16–19] is applied to obtain a series of interatomic potentials related to $Ce_{1-x}Sc_xFe_4Al_8$ from the first-principle cohesive energy calculation. Based on these calculated potentials, the preferential distribution of Fe in $CeFe_4Al_8$ alloys is calculated first. Then with Sc atoms substituting for Ce, the lattice parameters of $Ce_{1-x}Sc_xFe_4Al_8$ are also evaluated. These are explorations for the structures of complex materials using the interatomic potentials. In addition, some simple mechanical properties are worked out. Particularly, it is the first attempt to obtain some lattice vibrational properties for quarternary intermetallic compounds with $ThMn_{12}$-type structure, which may be used to predict some relevant thermodynamic properties such as Debye temperature.

2. Lattice inversion method

Chen's inversion theorem [16–19] has been developing a rigorous and concise approach to obtain the interatomic pair potentials based on the ab initio cohesive energy. And it has been applied successfully to study the lattice dynamics [20,21], the field-ion microscopy image of Fe_3Al analysis [19,22], the site preference of ternary additions in Ni_3Al and

* Corresponding author. Tel./fax: +86-10-62772783.
E-mail address: kangyanmei@yahoo.com.cn (Y.-M. Kang).

0022-3697/03/$ - see front matter © 2002 Elsevier Science Ltd. All rights reserved.
PII: S0022-3697(02)00330-X

Fe_3Al [23,24], the phase stability of $Gd(Fe,T)_{12}$ [25] and so on. The method is introduced concisely as follows:

Suppose that the crystal cohesive energy can be expressed as the sum of interatomic pair potentials

$$E(x) = \frac{1}{2}\sum_{n=1}^{\infty} r_0(n)\Phi(b_0(n)x) \tag{1}$$

where x is the nearest-neighbor distance, $r_0(n)$ is the coordination number of nth neighbor, $b_0(n)x$ is the distance of nth neighbor, $b_0(1) = 1$. The series $\{b_0(n)\}$ can be extended into a multiplicatively closed semi-group $\{b(n)\}$. In $\{b(n)\}$, for any two integers m and n, there exists a sole integer k satisfying $b(k) = b(m)b(n)$. Then Eq. (1) can be written as

$$E(x) = \frac{1}{2}\sum_{n=1}^{\infty} r(n)\Phi(b(n)x) \tag{2}$$

where

$$r(n) = \begin{cases} r_0(b_0^{-1}[b(n)]) & \text{if } b(n) \in \{b_0(n)\} \\ 0 & \text{if } b(n) \notin \{b_0(n)\} \end{cases} \tag{3}$$

and the pair potential from inversion can be written as

$$\Phi(x) = 2\sum_{n=1}^{\infty} I(n)E(b(n)x) \tag{4}$$

where $I(n)$ is determined by

$$\sum_{b(n)|b(k)} I(n)r\left(b^{-1}\left[\frac{b(k)}{b(n)}\right]\right) = \delta_{k1} \tag{5}$$

It is noted that $I(n)$ is related only to crystal geometrical structure, not to concrete element category, i.e. $\{I(n)\}$ is uniquely determined by $\{r_0(n)\}$ and $\{b_0(n)\}$. With the contribution of the interatomic potentials between the identical atoms subtracted from the total cohesive energy, the partial cohesive energy of the distinct atoms is obtained, and the interatomic potentials between the distinct atoms are determined by the lattice inversion [17,18].

In principle, all interatomic pair potentials can be obtained by strict lattice inversion from cohesive energy that can be evaluated from direct ab initio calculation without any experimental data. In this work, the calculations of $E(x)$ are performed on the basis of an ab initio augmented-spherical-wave method [26–28] within the local density functional theory. A detailed description of the ab initio calculation and the parameters is given in Appendix A. It is found that the converted data for the interatomic potentials can be approximately expressed as Morse function

$$\Phi(R) = D_0\{\exp[-2\alpha(R - R_0)] - 2\exp[-\alpha(R - R_0)]\}$$

where R is the distance between two atoms, D_0, α, R_0 are the parameters. The calculated interatomic potentials Φ_{Ce-Ce}, Φ_{Ce-Sc}, Φ_{Ce-Fe}, Φ_{Ce-Al}, Φ_{Sc-Sc}, Φ_{Sc-Fe}, Φ_{Sc-Al}, Φ_{Fe-Fe}, Φ_{Fe-Al}, Φ_{Al-Al} are shown in Fig. 1.

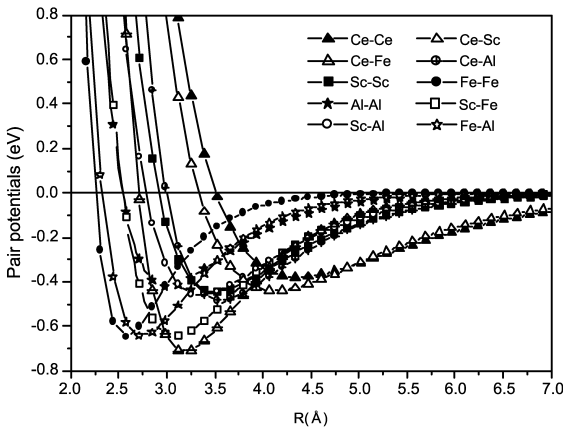

Fig. 1. Potentials of Ce–Sc–Fe–Al.

3. Preferential site occupation of Fe

Despite the structure of $CeAl_{12}$ being metastable, it can be considered the intrinsic structure of $CeFe_4Al_8$. In a typical crystal cell with two RAl_{12} molecular formulas (26 atoms per unit cell), there are three nonequivalent sites 8i, 8j, 8f for Al atoms and one site 2a for rare-earth atoms (Fig. 2). The sample system is chosen $(CeAl_{12})_{250}$ as crystal cell with periodic boundary in order to reduce statistical fluctuation and relaxed under the interaction of pair potentials using the conjugate gradient method with the cut-off radius of 14 Å. The energy values for $CeFe_4Al_8$ in Table 1 are the results of the arithmetic average for 100 samples produced by Fe atoms randomly distributed over the 8i, 8j, 8f, 8i + 8j, 8i + 8f, 8j + 8f and 8i + 8j + 8f sites, respectively. It shows obviously that the cohesive energy is lower when Fe atoms are substituted for Al atoms at the 8f sites than that for ones at the 8i and 8j sites. It indicates that Fe atoms prefer the 8f sites and Al atoms reside in the 8i and

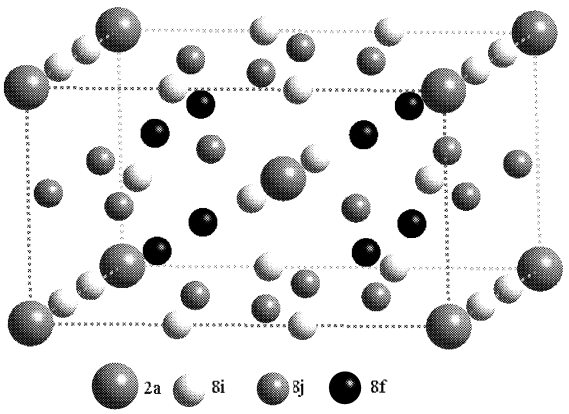

Fig. 2. Crystal structure of $ThMn_{12}$-type compound.

Table 1
Calculated cohesive energy of $CeFe_4Al_8$ while Fe atoms distributed over different sites

Site	8i	8j	8f	8i + 8j	8i + 8f	8j + 8f	8i + 8j + 8f
Energy (eV/atom)	−4.224	−4.485	−4.595	−4.377	−4.400	−4.513	−4.412

8j sites by the energy criterion when $x = 4$. The results are agreement with experiments [29,30].

4. Lattice constants and cohesive energies of $Ce_{1-x}Sc_xFe_4Al_8$

In the calculation procedure, the initial lattice constants of $CeFe_4Al_8$ are chosen arbitrarily in a certain range. After the energy minimization, the final structure can stabilize to tetragonal with space group *I*4/*mmm* within the tolerance 0.1 Å. The lattice constants are $a = 8.902$ Å, $c = 5.013$ Å (Table 2), which are close to the experimental data [7,15,30,31]. A certain range randomness of the initial structure and the stability of the final structure illustrate that the interatomic pair potentials are valid to study the material structural properties.

According to the stabilized structure of $CeFe_4Al_8$ obtained from the above calculation, the supercell $(CeFe_4Al_8)_{250}$ is applied to evaluate the lattice parameters and cohesive energies for $Ce_{1-x}Sc_xFe_4Al_8$. In the calculations, the model of $Ce_{1-x}Sc_xFe_4Al_8$ is constructed with Sc atoms substituting randomly for Ce at the 2a sites. The configuration average is taken for 100 samples for each Sc content. The calculated lattice constants are listed in Table 3 and the cohesive energy values in Fig. 3.

From Table 3, one can find that the calculated lattice constants of $Ce_{1-x}Sc_xFe_4Al_8$ ($0 \le x \le 1$) are in agreement with experimental results. The lattice constants both a and c decrease with the content of Sc, and the former is larger while the latter is a little smaller than the experimental data. The average deviation for a is 1.435% with the largest 2.310% from the experiment and that for c is 0.891% with the largest 1.477%. For the calculated volume of per unit of $Ce_{1-x}Sc_xFe_4Al_8$ the average error is 1.975%. In the calculation, it is assumed that $Ce_{1-x}Sc_xFe_4Al_8$ has a relatively perfect periodic crystal structure and four Fe atoms entirely distribute over the 8f sites. In fact for RT_4Al_8 the 8f sites are the majority sites for T atoms, but a small amount of sites are also for Al atoms [30,33]. In addition, the stoichiometry of RT_4Al_8 exhibits the compositions different from 1:4:8 ratio even single crystals of these materials [8,34]. These may result in the deviation of the calculations from the experimental data.

Fig. 3 shows the dependence of the cohesive energy for $Ce_{1-x}Sc_xFe_4Al_8$ on the Sc content. With increasing the content of Sc, the cohesive energy firstly decreases to a lowest value when x is between 0.2 and 0.3, and then increases. This curve can be analyzed qualitatively from the interaction potentials in Fig. 1. There are six kinds of interaction potentials about $CeFe_4Al_8$, i.e. Φ_{Ce-Ce}, Φ_{Ce-Fe}, Φ_{Ce-Al}, Φ_{Fe-Fe}, Φ_{Fe-Al} and Φ_{Al-Al}. With Sc atoms partially substituting for Ce atoms, four additional interatomic potentials Φ_{Ce-Sc}, Φ_{Sc-Sc}, Φ_{Sc-Fe} and Φ_{Sc-Al} are included into the system. When Sc atoms substitute all Ce atoms, the interatomic potentials related to the system are Φ_{Sc-Sc}, Φ_{Sc-Fe}, Φ_{Sc-Al}, Φ_{Fe-Fe}, Φ_{Fe-Al} and Φ_{Al-Al}. So the variation of the system energy is mainly determined by the difference between Φ_{Ce-Ce} and Φ_{Ce-Sc}, Φ_{Ce-Ce} and

Table 2
Crystal constants of $CeFe_4Al_8$

Initial states			Final states		
a, b, c (Å)	α, β, γ (deg)	Space group	a, b, c (Å)	α, β, γ (deg)	Space group
2.5, 2.5, 1.25	90, 90, 90	*I*4/*mmm*	8.902, 8.902, 5.013	90, 90, 90	*I*4/*mmm*
18, 18, 10	90, 90, 90	*I*4/*mmm*	8.902, 8.902, 5.013	90, 90, 90	*I*4/*mmm*
9, 9, 5	80, 70, 130	$P\bar{1}$	8.902, 8.902, 5.013	90, 90, 90	*I*4/*mmm*
2.5, 2.5, 1.25	50, 50, 50	*C*2/*m*	8.902, 8.902, 5.013	90, 90, 90	*I*4/*mmm*
15, 15, 7.5	110, 90, 80	$P\bar{1}$	8.902, 8.902, 5.013	90, 90, 90	*I*4/*mmm*
3, 3, 4	120, 80, 70	$P\bar{1}$	8.902, 8.902, 5.013	90, 90, 90	*I*4/*mmm*
16, 9.5, 10	70, 80, 110	$P\bar{1}$	8.902, 8.902, 5.013	90, 90, 90	*I*4/*mmm*
3, 12, 7	80, 80, 70	$P\bar{1}$	8.902, 8.902, 5.013	90, 90, 90	*I*4/*mmm*
16, 6.5, 4	70, 70, 70	$P\bar{1}$	8.902, 8.902, 5.013	90, 90, 90	*I*4/*mmm*
3, 4, 10	80, 80, 65	$P\bar{1}$	8.902, 8.902, 5.013	90, 90, 90	*I*4/*mmm*
14, 15, 8	80, 95, 130	$P\bar{1}$	8.902, 8.902, 5.013	90, 90, 90	*I*4/*mmm*
20, 25, 22.5	40, 60, 50	$P\bar{1}$	12.661, 20.174, 21.622	20.9, 28.1, 12.8	*P*1

Table 3
The comparison between the calculated and experimental [15] lattice parameters a and c for $Ce_{1-x}Sc_xFe_4Al_8$

x	a			c		
	Cal. (Å)	Exp. (Å)	Err. (%)	Cal. (Å)	Exp. (Å)	Err. (%)
0	8.902	8.826 (8.770[a]) (8.805[b]) (8.793[c])	0.861 (1.505[a]) (1.102[b]) (1.240[c])	5.013	5.060 (5.023[a]) (5.048[b]) (5.047[c])	0.929 (0.199[a]) (0.693[b]) (0.674[c])
0.1	8.891	8.807	0.954	5.005	5.06	1.087
0.3	8.872	8.779	1.059	4.991	5.043	1.031
0.5	8.854	8.734	1.374	4.976	5.022	0.916
0.7	8.837	8.700	1.575	4.960	5.017	1.136
0.9	8.822	8.661	1.859	4.943	5.011	1.357
1	8.815	8.647 (8.616[d])	1.943 (2.310[d])	4.935	5.009 (4.950[d])	1.477 (0.303[d])

[a] Ref. [7].
[b] Ref. [31].
[c] Ref. [30].
[d] Ref. [32].

Φ_{Sc-Sc}, Φ_{Ce-Fe} and Φ_{Sc-Fe} as well as Φ_{Ce-Al} and Φ_{Sc-Al}. The detailed analysis is as follows.

(1)(a) As can be seen in Fig. 4, the $\Phi_{Ce-Ce}(r)$ intersects $\Phi_{Ce-Sc}(r)$ at $r = 4.9$ Å. For $r \geq 4.9$ Å, these two potential curves coincide with each other. In the range $r < 4.9$ Å, with Sc substituting for Ce, the system energy will decrease due to $\Phi_{Ce-Sc}(r) < \Phi_{Ce-Ce}(r)$. The distances from Ce to its nearest and next-nearest Ce and Sc atoms are 5.013 and 6.775 Å, which are larger than 4.9 Å. So, the effect of the difference between $\Phi_{Ce-Sc}(r)$ and $\Phi_{Ce-Ce}(r)$ on the system energy can be neglected.

(b) The $\Phi_{Ce-Ce}(r)$ intersects $\Phi_{Sc-Sc}(r)$ at $r = 4.0$ Å. When the interatomic distance $r > 4.0$ Å, $\Phi_{Ce-Ce}(r) < \Phi_{Sc-Sc}(r)$, i.e. Sc substituting for Ce will result in the increasing of the system energy. From (1)(a), the distance between Ce and its nearest and next-nearest atoms is larger than 4.0 Å, so the system energy increases in this case.

(2) The $\Phi_{Ce-Fe}(r)$ intersects $\Phi_{Sc-Fe}(r)$ at $r = 2.97$ Å (Fig. 5). When the interatomic distance $r < 2.97$ Å, $\Phi_{Sc-Fe}(r) < \Phi_{Ce-Fe}(r)$; $2.97 \leq r \leq 4.4$ Å, $\Phi_{Sc-Fe}(r) > \Phi_{Ce-Fe}(r)$; and $r > 4.4$ Å, $\Phi_{Ce-Fe}(r) \approx \Phi_{Sc-Fe}(r)$. The distance between Ce and its next-nearest Fe atoms is 4.903 Å, which is larger than 4.4 Å, so the system energy will not change for the Sc substitution for Ce. While the distances between Ce and its eight nearest Fe atoms are 3.388 Å, so the energy will increase due to $\Phi_{Ce-Fe}(r) < \Phi_{Sc-Fe}(r)$ in this range.

(3) For $\Phi_{Ce-Al}(r)$ and $\Phi_{Sc-Al}(r)$, they intersect at $r = 3.4$ Å (Fig. 6). If the interatomic distance $r < 3.4$ Å, $\Phi_{Sc-Al} < \Phi_{Ce-Al}$; if $r > 5.5$ Å, $\Phi_{Sc-Al} \approx \Phi_{Ce-Al}$; if 3.4 Å $\leq r \leq 5.5$ Å, $\Phi_{Sc-Al} > \Phi_{Ce-Al}$. (a) The distances between Ce and its nearest four Al atoms at the 8i site and eight Al atoms at the 8j site are 3.15 and 3.2 Å, respectively. So considering the nearest neighbor interaction alone, the energy will decrease when Sc is substituted for Ce. (b) The distance between Ce and its next-nearest 16 Al atoms at the 8i site and eight Al atoms at the 8j site are 5.272 and 5.086 Å, respectively,

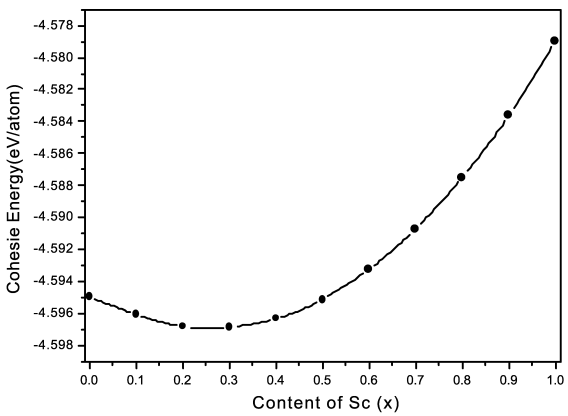

Fig. 3. Calculated cohesive energy of $Ce_{1-x}Sc_xFe_4Al_8$ after relaxation.

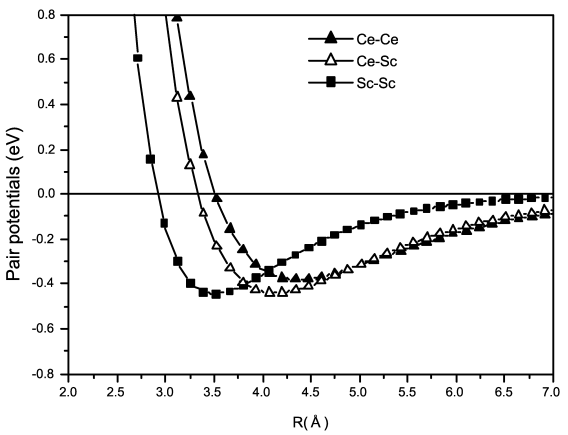

Fig. 4. Potentials of Ce–Ce, Ce–Sc and Sc–Sc.

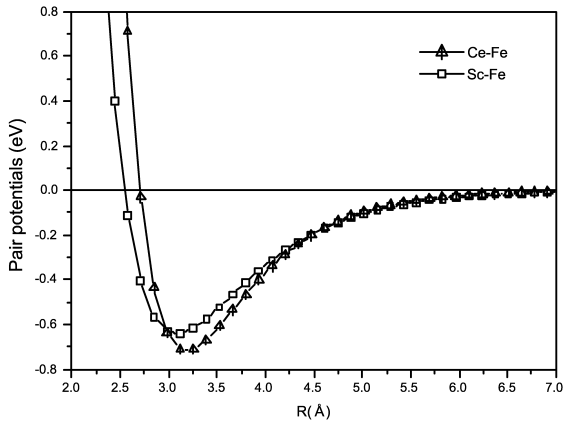

Fig. 5. Potentials of Ce–Fe and Sc–Fe.

which are within 3.4–5.5 Å, so the energy increases with Sc substituting for Ce.

In summary, the case of (3)(a) induces the system energy to decrease, while the cases of (1)(b), (2) and (3)(b) all result in the increasing of the energy. The latter plays a more important role than the former. This does not seem to explain the energy decreases when a small amount of Sc atoms are substituted for Ce atoms. In fact, the rate that two Sc atoms are nearest-neighbors is almost zero when a few of Sc atoms exist in the system. So at this case the system energy is mainly influenced by (3)(b) instead of (1)(b), which results in the decreasing of the system energy. However, with the content of Sc atoms, (1)(b) will play a more significant role in increasing the system energy. So the system energy has a lowest value when Sc content is small, and then increases.

It is noted that there is a little change of the system energy with the content of Sc. This may explain the $Ce_{1-x}Sc_xFe_4Al_8$ compound always exists whatever x is.

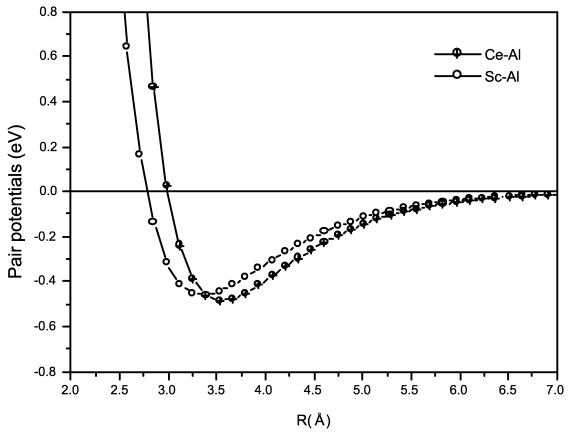

Fig. 6. Potentials of Ce–Al and Sc–Al.

Table 4
The elastic constants C_{ij} and bulk modulus for $Ce_{1-x}Sc_xFe_4Al_8$

x	Elastic constants C_{ij} (GPa)						Bulk modulus (GPa)
	C_{11}	C_{12}	C_{13}	C_{33}	C_{44}	C_{66}	
0	432	62	116	411	92	63	206.78
0.1	431	64	116	413	93	65	207.50
0.3	426	68	117	411	94	67	207.03
0.5	421	72	117	411	95	69	206.95
0.7	417	76	117	412	96	71	206.81
0.9	413	79	116	413	97	73	206.52
1	411	81	116	413	97	74	206.33

5. Elastic constants and bulk moduli for $Ce_{1-x}Sc_xFe_4Al_8$

Generally for the rare earth compounds it is difficult to measure the mechanical properties experimentally because of their brittleness. And huge computer resource is required with ab initio method due to their complex structure. In this work the elastic constants and the bulk moduli of $Ce_{1-x}Sc_xFe_4Al_8$ ($0 \le x \le 1$) are evaluated by the inverted pair potentials. The results are listed in Table 4.

As Table 4 shows, the values of the components of the elastic modulus increase for C_{12}, C_{44} and C_{66} and decrease for C_{11}, for C_{13} and C_{33} there is no obvious change with the Sc content. In addition, the bulk moduli for $Ce_{1-x}Sc_xFe_4Al_8$ change slightly with the content of Sc.

6. Phonon densities of states of $Ce_{1-x}Sc_xFe_4Al_8$ ($x = 0$, 0.5, 1)

Phonon density of states (DOS) reflects the lattice dynamic properties, from which some important thermodynamic parameters such as specific heat, vibrational entropy and Debye temperature can be derived. Generally, the phonon spectra are measured by an inelastic neutron scattering technique. Then fit the interatomic force constants to the experimental data by constructing an empirical model or determine the force constants by the first-principle calculations. For the rare earth compounds, due to the low symmetry of the complex structure and the necessity to involve many parameters in any approach, it is difficult to calculate and measure their phonon spectra.

In this section, with the inverted interatomic potentials, the total phonon densities of states as well as the partial DOS of different elements for $Ce_{1-x}Sc_xFe_4Al_8$ ($x = 0$, 0.5, 1) are evaluated in a crystal cell including 26 atoms based on the lattice theory. The results of $CeFe_4Al_8$, $ScFe_4Al_8$ and $Ce_{0.5}Sc_{0.5}Fe_4Al_8$ are shown in Figs. 7–9. The highest frequencies of these materials are 14.0, 15.1 and 14.6 THz, respectively. For the density of the states of $CeFe_4Al_8$, there are four apexes around 3.0, 5.0, 7.0 and 10.5 THz and two

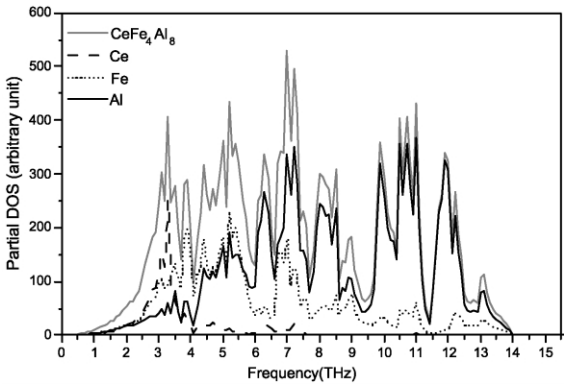

Fig. 7. Phonon DOS of $CeFe_4Al_8$.

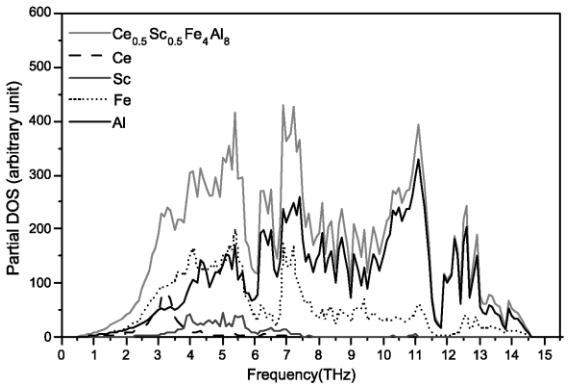

Fig. 9. Phonon DOS of $Ce_{0.5}Sc_{0.5}Fe_4Al_8$.

localized modes whose frequencies are higher than 11.0 THz. The ratio of the modes contributed by Ce, Fe and Al is 1:4:8 in the total frequency range. However, Ce contributes a major part to the modes with lower frequencies. In the range of 9.5–14.0 THz, the modes are mostly excited by Al atoms and are much more than those by Fe atoms and the ratio of the former to the latter is approximate 7:1.

Considering the nearest neighbors, one can analyze qualitatively the vibrational modes from interaction potentials (Fig. 1). There are four Al atoms at the 8i site and eight Al at the 8j site around Ce. The distances between Ce and these atoms are 3.15 and 3.20 Å for the relaxed structure. As shown in Fig. 1, Ce reacts strongly with Al at these distances. The mass of Ce is much larger than that of Al, so it is assumed motionless relative to Al atom. Then some of Al atoms are restricted in the 'potential well' $\Phi_{Ce-Al}(r)$. This might be the reason for appearance of the localized modes of Al atoms, which corresponds to higher transected frequency. For Fe atom, there are the same cases with that of Al. Furthermore, the distances between Fe and its nearest four Al atoms at the 8i site and four Al at the 8j site are 2.72 and 2.57 Å, respectively. Since the curve $\Phi_{Fe-Al}(r)$ is deep and narrow, Fe also reacts strongly with these Al atoms, which may contribute the higher frequency modes due to light mass of Al. In addition, though the interaction between Ce and Fe is intense at their nearest distance (3.39 Å), Fe atoms cannot be excited more modes with higher frequency than Al atom due to the heavy mass of Fe.

For the phonon spectrum of $ScFe_4Al_8$, there are three apexes around 5.0, 7.5 and 11.0 THz, respectively, and two localized modes whose frequencies are higher than 12.2 THz. The ratio of the modes excited by Sc, Fe and Al is 1:4:8 in the total frequency range. Comparing Figs. 7 and 8, one can see hat the contributions of Fe and Al atoms to the total DOS of $ScFe_4Al_8$ are similar with those of $CeFe_4Al_8$ because there is little difference in the structures and the distances between the distinct atoms for these two materials. However, the apex of the contribution of Sc is about 5.0 THz, which is larger than that of Ce (3.0 THz). So the first apex in the phonon spectra of $CeFe_4Al_8$, which mainly contributed by Ce, disappears instead the apex at 5.0 THz comes out in that of $ScFe_4Al_8$. However, the intensity of the localized modes for $CeFe_4Al_8$ is larger than that of $ScFe_4Al_8$. This can be explained by the creations of the localized modes. As discussed for $CeFe_4Al_8$, the localized modes are mainly created by the strong interaction

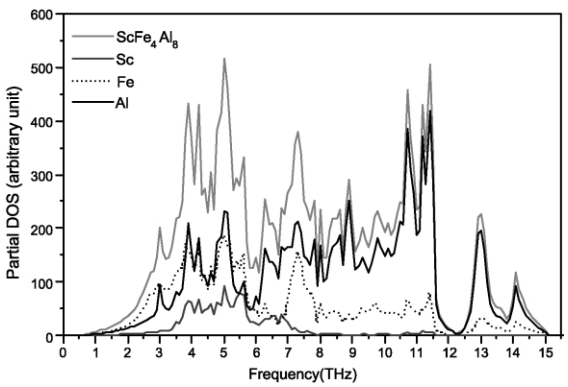

Fig. 8. Phonon DOS of $ScFe_4Al_8$.

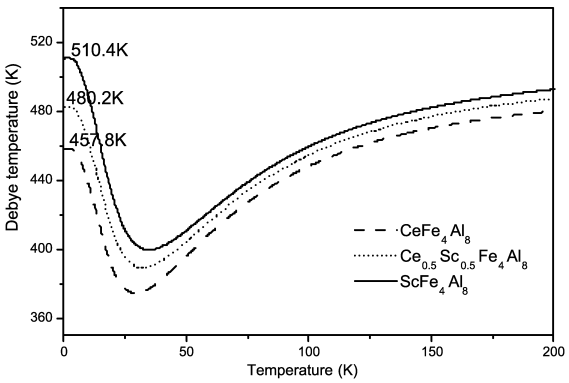

Fig. 10. The dependence of the Debye temperature on the temperature for $CeFe_4Al_8$, $Ce_{0.5}Sc_{0.5}Fe_4Al_8$ and $ScFe_4Al_8$.

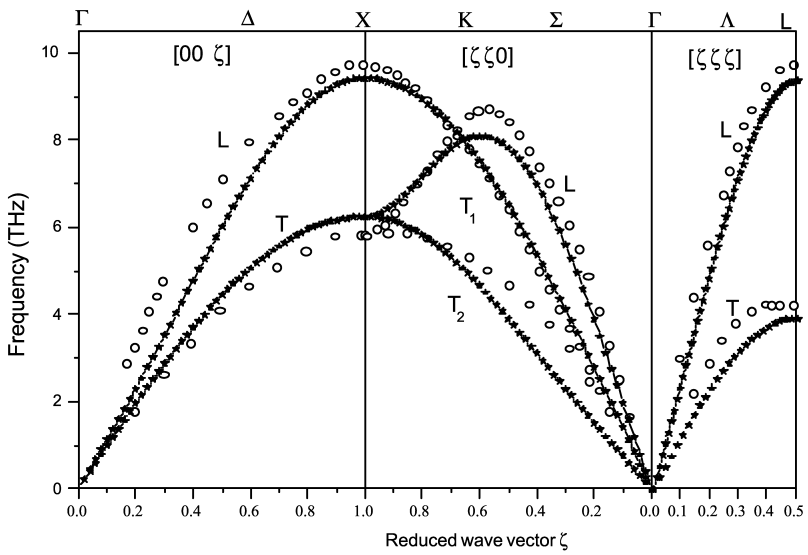

Fig. 11. Comparison of the calculated and experimental phonon dispersion for Al. Circles represent experimental data [35].

of Fe and Al as well as Sc and Al. However, the interaction between Ce and Al at 3.15 and 3.20 Å is stronger than that between Sc and Al at 3.09 and 3.12 Å. And the mass of Ce is much heavier than that of Sc. These two conditions cases induce more modes with higher frequencies excited by Al in $CeFe_4Al_8$ than in $ScFe_4Al_8$.

For the DOS of the compound $Ce_{0.5}Sc_{0.5}Fe_4Al_8$ there are three apexes at the similar distances with $ScFe_4Al_8$. Its first apex is expended relative to that of the latter. Four apexes appear in the localized modes. It may result from the combination of interactions of Ce–Al and Sc–Al besides the interaction of Fe–Al. With the above analysis for the densities of states of $CeFe_4Al_8$ and $ScFe_4Al_8$, it is easy to understand those of $Ce_{0.5}Sc_{0.5}Fe_4Al_8$ from the interaction potentials shown in Fig. 1.

Furthermore, the Debye temperature of a material is a suitable parameter to describe phenomena of solid-state physics that are associated with lattice vibrations. In this paper, the dependences of the Debye temperature on the temperature for $CeFe_4Al_8$, $Ce_{0.5}Sc_{0.5}Fe_4Al_8$ and $ScFe_4Al_8$ are derived from the calculated phonon DOS. The results are shown in Fig. 10. The values are 457.8, 480.2 and 510.4 K near 0 K, respectively, that is, the Debye temperature increases with the content of Sc. However, so far, the above calculations have not been verified by experiments.

At last the phonon dispersions of Al atom, which takes up a large proportion in $Ce_{1-x}Sc_xFe_4Al_8$, are worked out using the same potentials as in the above compounds. The calculated results along the three main symmetry directions [001], [110] and [111] zone and the experimental data [35] are plotted in Fig. 11. In addition, the phonon DOS of Al is also evaluated. It is shown in Fig. 12 and the results from an eight neighbor Born–von Karman model fitted to elastic constants and symmetry and off symmetry phonons

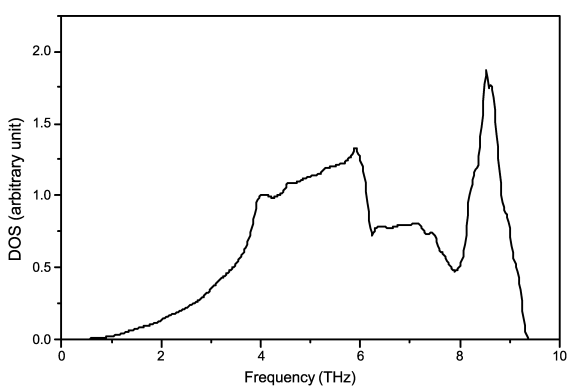

Fig. 12. Phonon spectrum calculated from the inverted potentials.

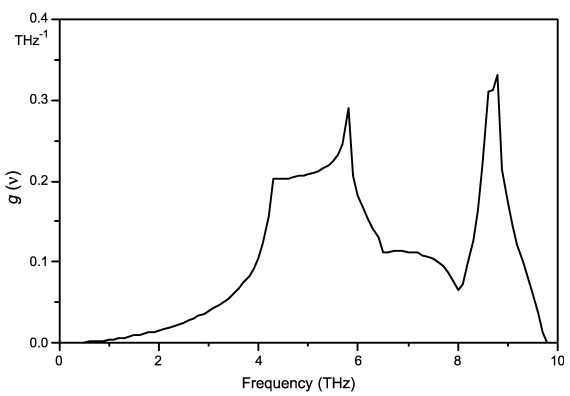

Fig. 13. Phonon spectrum calculated from an eight neighbor Born–von Karman model fitted to elastic constants and symmetry and off symmetry phonons experiments [36].

experiments [36] in Fig. 13. From Figs. 11 and 13, it can be seen that the results employing the inverted potentials in this work are agreement with the experimental data.

7. Conclusion and discussion

In this work the distribution of Fe in $CeFe_4Al_8$ is evaluated by using the interatomic potentials. The calculated result demonstrates that Fe atoms occupy preferentially the 8f sites and Al atoms reside in the 8i and 8j sites. This is in good agreement with experiments. Besides, the calculated lattice constants for $Ce_{1-x}Sc_xFe_4Al_8$ ($0 \le x \le 1$) also agree with the experimental data very well and the percentage difference between experiment and calculation is about 2%. All the above results show that our lattice converted interatomic potentials are suitable to describe these rare-earth intermetallics. Now let us go a step further; these potentials are applied to evaluate phonon DOS of $Ce_{1-x}Sc_xFe_4Al_8$ ($x = 0$, 0.5, 1) and the dependence of the Debye temperature on the temperature in the range of 0–200 K for the first time. Although generally pair potentials have inherent drawbacks, which induce a false Cauchy relation and almost hardly deal with the anisotropic properties, they can reproduce cohesive energy, lattice constants, bulk modulus and some other simple properties very well. In summary, the method using the inverted potentials is effective to investigate the site preference, phase stability and to predict the mechanical and thermodynamic properties for these materials with complex structures. On the other hand, there are difficulties in solving the problems such as solubility and occupation fraction due to the fact that the entropy and temperature are not taken into account. This remains for future study.

Acknowledgments

This work is supported in part by the National Nature Science Foundation of China, No 59971006 and in part by the National Advanced Materials Committee of China and Special Funds for Major State Basic Research of China, No. G2000067101 and No. G2000067106.

Appendix A. Ab initio calculated parameters for the cohesive energy

In this work, the total energy *ab initio* caculations are performed with the ESOCS 4.0 program provided by Materials Simulation Incorporation. The cohesive energy is obtained from

$$E(x) = E_{tot}(x) - E_{tot}(\infty)$$

A series of functions $E(x)$ are calculated with various lattice constants at equal intervals of 0.1 Å. In each case, for generating the total energy, more than 80 k-points in an irreducible Brillouin zone are taken into account in a self-consistent calculation. The partial cohesive energy of the distinct atoms is obtained by subtracting the contribution of identical atoms from the total cohesive energy. For example, the partial cohesive energy of Ce–Al is obtained as follows:

$$E_{\mathrm{Ce-Al}}(x) = E^{B_2}_{\mathrm{Ce-Al}}(x) - E^{SC}_{\mathrm{Ce}}(x) - E^{SC}_{\mathrm{Al}}(x)$$

$$= \sum_{i,j,k\neq 0}^{\infty} \Phi_{\mathrm{Ce-Al}}\left(\sqrt{\tfrac{4}{3}\left[\left(i-\tfrac{1}{2}\right)^2+\left(j-\tfrac{1}{2}\right)^2+\left(k-\tfrac{1}{2}\right)^2\right]}x\right)$$

where x is the nearest neighbor distance in B_2 structure, $E^{B_2}_{\mathrm{Ce-Al}}(x)$ represents the total energy curve with B_2 structure and $E^{SC}_{\mathrm{Sc}}(x)$, $E^{SC}_{\mathrm{Al}}(x)$ the total energy functions with simple cubic structures. The data are then fitted on the basis of Rose functions

$$E(x) = E_0(1 + x')\exp(-x')$$

$$\text{with } x' = \sqrt{9(B_0V_0/E_0)}(x/a_0 - 1)$$

where a_0 and E_0 are the equilibrium lattice constant and cohesive energy respectively, B_0 the bulk modulus, and V_0 the equilibrium atomic volume. The calculated cohesive energies used to obtain directly the potentials of the identical atoms and distinct atoms are listed in the following table.

Ab initio calculated parameters for the cohesive energy

Object	a_0 (Å)	B_0 (10^{12} dyn/cm^2)	E_0 (eV)	Object	a_0 (Å)	B_0 (10^{12} dyn/cm^2)	E_0 (eV)
Ce	5.160	0.239	−4.320	Ce–Fe	3.618	0.585	−6.087
Sc	4.549	0.524	−3.885	Ce–Al	4.017	0.261	−4.183
Fe	2.745	2.965	−4.427	Sc–Fe	3.414	0.454	−5.903
Al	4.006	0.821	−3.386	Sc–Al	3.735	0.261	−4.161
Ce–Sc	4.426	0.118	−4.395	Fe–Al	3.111	0.795	−5.517

References

[1] K.H.J. Buschow, J. Appl. Phys. 63 (1988) 3130.
[2] K. Ohashi, Y. Tawara, R. Osugi, J. Sakurai, Y. Komura, J. Less-Common Met. 139 (1988) L1.
[3] B.P. Hu, K.Y. Wang, Y.Z. Wang, Z.X. Wang, Q.W. Yan, P.L. Zhang, X.D. Sun, Phys. Rev. B 51 (1995) 2905.
[4] V.Yu. Bodriakov, T.I. Ivanova, S.A. Nilitin, I.S. Tereshina, J. Alloys Compd 259 (1997) 265.
[5] G. Bonfait, M. Godinho, P. Estrela, A.P. Gonçalves, M. Almeida, J.-C. Spirlet, Phys. Rev. B 53 (1996) R480.
[6] K. Pećko, M. Biernacka, L. Dobrzyńska, D. Satuła, K. Szymański, J. Waliszewski, W. Suski, K. Wochowski, G. André, F. Bourée, J. Phys.: Condens. Matter 9 (1997) 9541.
[7] P. Schobinger-Papamantellos, K.H.J. Buschow, C. Ritter, J. Magn. Magn. Mater. 186 (1998) 21.
[8] M. Kuznietz, A.P. Gonçalves, J.C. Waerenborgh, M. Almeida,

C.C. Cardoso, M.M. Cruz, M. Godinho, Phys. Rev. B 60 (1999) 9494.
[9] J.A. Paixão, M. Ramos Silva, S.Aa. Sørensen, B. Lebach, G.H. Lander, P.J. Brown, S. Langridge, E. Talik, A.P. Gonçalves, Phys. Rev. B 61 (2000) 6176.
[10] P. Gaczyński, F.G. Vagizov, W. Suski, B. Kotur, W. Iwasieczko, H. Drulis, J. Magn. Magn. Mater. 225 (2001) 351.
[11] K.H.J. Buschow, A.M. van Kraan, J. Phys. F8 (1978) 921.
[12] I. Felner, I. Nowik, M. Seh, J. Magn. Magn. Mater. 38 (1983) 172.
[13] P.C.M. Gubbens, A.M. van der Kraan, K.H.J. Buschow, J. Magn. Magn. Mater. 27 (1982) 61.
[14] W. Suski, B. Kotur, K. Wochowski, Physica B 281 (2000) 81.
[15] P. Gaczyński, F.G. Vagizov, W. Suski, B. Kotur, K. Wochowski, H. Drulis, J. Magn. Magn. Mater. 214 (2000) 37.
[16] N.X. Chen, Phys. Rev. Lett. 64 (1990) 1193.
[17] N.X. Chen, Z.D. Chen, Y.C. Wei, Phys. Rev. E 55 (1997) R5.
[18] W.Q. Zhang, Q. Xie, X.J. Ge, N.X. Chen, J. Appl. Phys. 82 (1997) 578.
[19] N.X. Chen, X.J. Ge, W.Q. Zhang, F.W. Zhu, Phys. Rev. B 57 (1998) 14203.
[20] M. Li, N.X. Chen, Phys. Rev. B 52 (1995) 997.
[21] S.J. Liu, S.Q. Duan, B.K. Ma, Phys. Rev. B 58 (1998) 9705.
[22] X.J. Ge, N.X. Chen, J. Appl. Phys. 85 (1999) 3488.
[23] J. Shen, Y. Wang, N.X. Chen, Y. Wu, Prog. Nat. Sci. 10 (2000) 457.
[24] X.D. Ni, N.X. Chen, J. Shen, J. Mater. Res. 16 (2001) 344.
[25] N.X. Chen, J. Shen, X.P. Su, J. Phys.: Condens. Matter 13 (2001) 2727.
[26] H.J. Monkhorst, J.D. Pack, Phys. Rev. B 13 (1976) 5188.
[27] A.R. Williams, J. Kuebler, J.R. Gelatt, Phys. Rev. B 19 (1979) 6094.
[28] V.L. Moruzzi, C.B. Sommers, Calculated Electronic Properties of Ordered Alloys, World Scientific, Singapore, 1995.
[29] W. Suski, in: K.A. Gschneidner Jr., L. Eyring (Eds.), Handbook on the Physics and Chemistry of Rare Earth, vol. 22, Elsevier, Amsterdam, 1996, pp. 162, Chapter 149.
[30] I. Felner, I. Nowik, J. Phys. Chem. Solids 39 (1978) 951.
[31] K.H.J. Buschow, J.H. van Vuch, T.W.W. van den HooGenhof, J. Less-Common Met. 50 (1976) 145.
[32] B.Yu. Kotur, D. Badurski, W. Suski, K. Wochowski, A. Gilewski, T. Mydlarz, Physica B 254 (1998) 107.
[33] O. Moze, R.M. Ibberson, R. Caciuffo, K.H.J. Buschowo, J. Less-Common Met. 166 (1990) 329.
[34] F.G. Vagizov, W. Suski, K. Wochowski, H. Drulis, J. Alloys Compd 219 (1995) 271.
[35] R. Stedman, G. Nilsson, Phys. Rev. 145 (1966) 492.
[36] E.R. Cowley, Can. J. Phys. 52 (1974) 1714.